Understanding the importance of Cu(I) intermediates in self-reducing molecular inks for flexible electronics

MARCHAL, Wouter; Longo, Alessandro; Briois, Valérie; Van Hecke, Kristof; ELEN, Ken; VAN BAEL, Marlies & HARDY, An (2018) Understanding the importance of Cu(I) intermediates in self-reducing molecular inks for flexible electronics. In: Inorganic chemistry, 57(24), p. 15205-15215.

DOI: 10.1021/acs.inorgchem.8b02493
Handle: http://hdl.handle.net/1942/27642

Understanding the importance of Cu(I) intermediates in self-reducing molecular inks for flexible electronics

Wouter Marchal[1,6], Alessandro Longo[2,3], Valérie Briois[4], Kristof Van Hecke[5], Ken Elen[1,6], Marlies K. Van Bael[1,6], An Hardy[1,6]

[1] UHasselt – Hasselt University, Institute for Materials Research (IMO-IMOMEC), Inorganic and Physical Chemistry, Agoralaan building D, 3950 Diepenbeek, Belgium
[2] European Synchrotron Radiation Facility, CS40220, Avenue des Martyrs 71, 38043 Grenoble Cedex 9, France
[3] UOS Palermo, CNR, ISMN, via Ugo La Malfa 153, 90146 Palermo, Italy
[4] Synchrotron SOLEIL, UR1-CNRS, L'Orme des Merisiers, Saint-Aubin, BP 48, 91192 Gif-Sur-Yvette Cedex, France
[5] XStruct, Ghent University, Department of Chemistry, Krijgslaan 281-S3, 9000 Ghent, Belgium
[6] Imec vzw, Division IMOMEC, Wetenschapspark 1, 3590 Diepenbeek, Belgium

Abstract

The fast and scalable low-temperature deposition of nanoscale metallic features is of the utmost importance for the development of future flexible smart applications including sensors, wireless communication and wearables. Recently, a new class of metalorganic decomposition (MOD) copper inks was developed, consisting of self-reducing copper formate containing amine complexes. From these novel inks, copper metal features with outstanding electrical conductivity (± 10 μΩ cm) are deposited at temperatures of 150 °C or less, which is well below the reduction temperature of orthorhombic α-copper formate (around 225 °C). However, the underlying principle of this reaction mechanism and the relationship between the corresponding temperature shift and the amine coordination is still under debate. The current study provides a full explanation for the shift in reduction temperatures via in-situ characterization. The results clearly indicate that the structural resemblance and stability of the Cu(II) starting compound and the occurring Cu(I) intermediate during the in-situ reduction, are the two main variables that rationalize the temperature shift. As such, the thermal compatibility of the copper MOD inks with conventional plastic substrates like polyethylene terephthalate (PET) can be explained, based on the metalorganic complex properties.

Introduction

The development of flexible electronics leans upon the availability of suitable metal inks which can be deposited in an easy, scalable way. These metal inks need to comply with many criteria: they should be non-toxic, compatible with the currently used printing techniques (screen printing, inkjet printing,…), stable, inexpensive and most of all curable at low temperatures to prevent degradation of the flexible substrates. Motivated by the substantial cost reduction, a shift in research focus from silver to copper metal inks can be easily understood from this economical, industry-driven context. Conventionally, metal inks are particle-based, which means the metal is already present in its reduced state, dispersed in a solvent blend and surrounded by capping agents, dispersants, surfactants, … This proven concept allows for the deposition of both silver and copper layers, using a wide variety of sintering/curing techniques [1-3]. Recently, the dawn of a second class of metal inks was witnessed, based on coordinated metal ions in solution containing ligands with a double function: stabilizing the metal ions in solution and acting as reductants during the precursor's decomposition. These inks can be categorized in the commonly known type of metalorganic decomposition precursors (MOD) [4]. One of the major advantages of these alternative inks is the absence of particles, greatly enhancing the ink stability and preventing operational difficulties during printing such as nozzle clogging due to coagulation in inkjet or spray-coating techniques. Very low sintering temperatures could be attained for silver inks [5], down to room temperature (RT) [6] as no high temperature boiling or decomposing organic components are present. MOD inks are easy to synthesize and compatible with many deposition and curing methods.

Also for copper, the MOD ink concept shows high potential for printable flexible electronics as a thermally initiated *in-situ* reduction can be performed below 150 °C [7-9]. Most of the reported copper MOD inks have a similar design: copper formate is coordinated to a variety of amine ligands yielding amine-formato-copper(II) coordination compounds, which are soluble in polar protic organic solvents such as simple alcohols and glycol ethers. Besides the 'pure' solution-based approach, copper MOD inks have been added to mixtures of metallic copper particles in hybrid inks, to serve as a conductive 'glue' between the particles after low-temperature sintering. In many cases, alkylamines (such as hexylamine) [10-13] or alkanolamines (such as 2-amino-methyl-1-propanol) [14-16] are employed as ligands. The *in-situ* reduction mechanism from Cu(II) to metallic copper relies on the self-reducible properties of the

copper formate salt itself. The formate anions are oxidized to carbon dioxide, thereby reducing the copper(II) at temperatures exceeding 200 °C, which is considerably higher than those of the corresponding amine complexes. This decomposition mechanism was studied before [17] and has been described as a complex interplay of different intermediate species, pointing to a step-wise reduction process [18]. Whereas all decomposition products are gasses (CO_2, H_2 plus CO and H_2O, from a possible side-reaction), and the amine ligand will readily evaporate in the targeted temperature range (100 - 150 °C), only metallic copper remains on the condition that the reaction is performed in inert atmosphere since the resulting copper metal would oxidize in ambient conditions otherwise. The general principle is illustrated in figure 1.

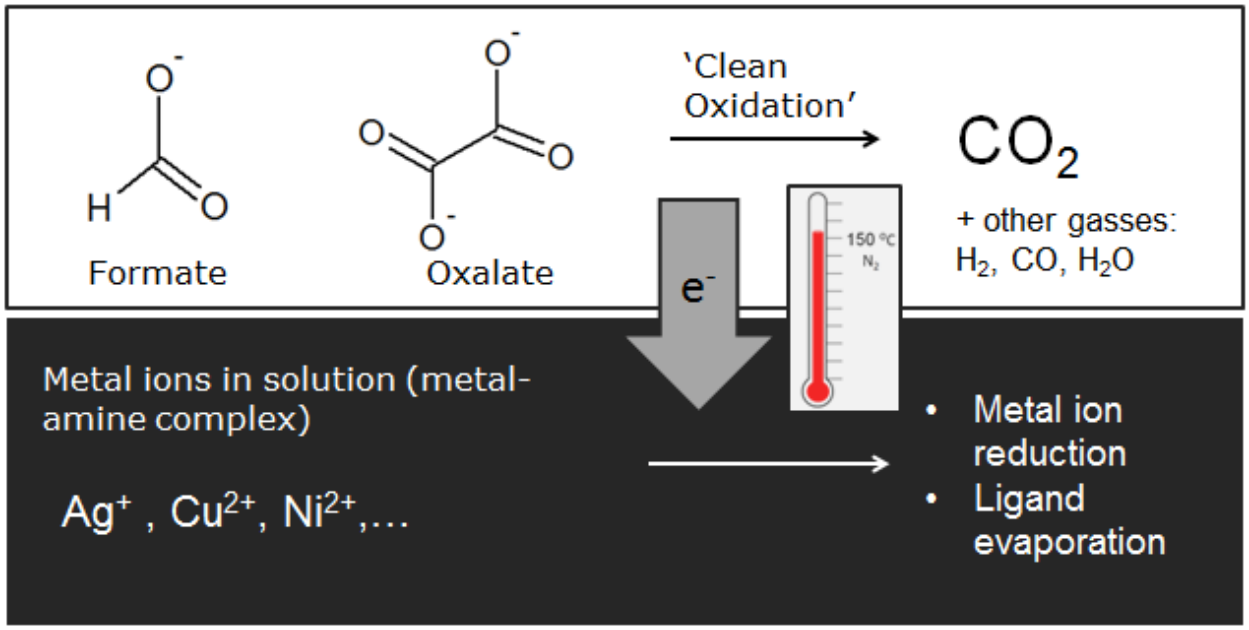

Figure 1: schematic representation of the MOD ink working principle. Reducing agents such as formate anions convert into carbon dioxide upon thermal activation and only gaseous products are formed: this can be labeled as a 'clean oxidation' as no organic residuals are left behind.

In the vast majority of the research papers devoted to copper MOD inks, the resulting layer properties regarding conductivity, roughness, adhesion or oxidation protection were emphasized [19-21]. However, less attention was devoted to the fundamental question why the applied amine complexes exhibited an *in-situ* reduction temperature which is up to 100 °C lower compared to the anhydrous copper formate salt, not to mention the possible formation of Cu(I) intermediates during this process. In order to explain the beneficial temperature shift upon amine coordination, different hypotheses have been put forward.

So far, *Shin et al*. [16] claimed that the coordinating alkanolamines themselves have mild reducing properties assisting the conversion from the divalent copper to the metallic state*, whereas* Farraj *et al.* [14] stated that water molecules interfere with the decomposition process of the complex and clearly indicated the occurrence of a Cu(I) intermediate. Choi *et al.* [10] explained the temperature shift by the electron-donating nature of the coordinating alkylamine, which would facilitate the release of the present carboxylate groups, and reducing properties of hexylamine. Eventually, Paquet *et al*. [22] reported a correlation between hydrogen bond formation properties between the amine and formate groups affecting sterical hindrance and the *in-situ* reduction temperature. Yet none of these hypotheses have been validated by an in-depth direct investigation of the reduction pathway. In this paper, we will critically address these claims and provide a generalized explanation for the observed temperature shift of the *in-situ* reduction of copper-alkylamine-formato complexes.

To unravel the fundamental reason for the temperature shift in copper formate-based MOD inks, a detailed study was performed on one of the most commonly reported copper MOD inks, being the copper-hexylamine-formato complex $Cu(hex)_2(HCOO)_2$. The starting compound structure was analyzed with extended X-ray absorption fine structure (EXAFS) measurements and compared to a set of crystalline reference structures analyzed with EXAFS and X-ray diffraction (XRD). Consequently, the thermal decomposition mechanisms were probed with *in-situ* X-ray absorption near edge structure (XANES) spectroscopy, -EXAFS and -XRD, supported with coupled thermogravimetric experiments (TG-FTIR and TG-MS). The data treatment was facilitated using statistical methods, including principal component analysis (PCA), multivariate curve regression alternating least squares (MCR-ALS) and linear combination analysis (LCA). Finally, the decomposition of the copper-hexylamine-formato complex is compared to a framework consisting of three other relevant compounds: a copper-pyridine-formato complex: $Cu(pyr)_2(HCOO)_2$, a copper-ethylenediamine-formato complex: $Cu(en)_2(HCOO)_2$ and the anhydrous α-copper formate salt. These reference compounds are selected based on the remarkable spread in their *in-situ* reduction temperatures and the possibility to obtain them as single crystalline compounds.

Materials and methods

Synthesis of copper complexes

Anhydrous copper formate was synthesized by adding copper nitrate trihydrate (12,0 g, Merck, pro analysis) to a 30 mL access of formic acid (Merck, 99%) at 60 °C while stirring in an open beaker under a closed fumehood. A vigourous reaction takes place, causing the evolution of brown NO_x fumes, proving the succesful conversion from the nitrate to the formate species. The pale blue residue is kept in an excess of formic acid at a temperature of 85 °C for 1 hour inside a large beaker. In these conditions, the conversion of $Cu(HCOO)_2.4HCOOH$ to the royal blue anhydrous $Cu(HCOO)_2$ takes place, as previously described by *Martin and Waterman [23],* for a similar synthetic route starting from copper carbonate. Stringent control of synthesis parameters is important given the polymorphic nature of copper formate anhydrate and the related dependency of the reaction product on the experimental conditions. Subsequently, the precipitate was filtered (Pall, supor-100, 0.1 micron) after cooling and washed with ethanol (absolute, VWR chemicals) and hexane (VWR chemicals). The residue was unambiguously identified as anhydrous copper formate, based on elemental CHN (Thermo electron flash EA1113 with BBOT calibration standard)- and thermogravimetric analysis (TGA, SDT, Q600 TA instruments) in nitrogen atmosphere (10 °C/min, 25°C – 400 °C, alumina sample pan), CHN: C% 15.02, N% 0.00, H% 1.3, TGA: Cu% 40.96.

The copper formate pyridine (pyr, Acros organics, 99+%), ethylenediamine (en, Alfa Aesar, 99%) and hexylamine (hex, Acros organics, 99%) complexes were obtained by adding 2 equivalents of the amine ligands to 0.768 g of copper formate after 2 mL of ethanol was already added to facilitate the coordination reaction and mixing of the MOD ink. Ethanol was selected on grounds of its limited ligation properties compared to the added amines, its capability to dissolve the copper hexylamine-formate complex to form a processable MOD ink and its low boiling point so the synthesized complexes can be easily dried. The following complexes were found after drying and the [Cu:Ligand] ratio of [1:2] could be confirmed in all cases: **$Cu(pyr)_2(HCOO)_2$**, CHN: C% 40.75, N% 7.74, H%, 4.22, TGA: Cu% 16.57, blue needle-like crystals. **$Cu(en)_2(HCOO)_2$**, CHN: C% 25.87, N% 19.31, H% 6.82, TGA: Cu% 24.41, purple crystals soluble in ethanol. **$Cu(hex)_2(HCOO)_2$,** CHN: C% 47.32, N% 8.71, H% 9.47, TGA: Cu% 17.46, indigo amorphous precipitate soluble in ethanol.

Characterization

For the characterization of the copper reduction potential in the studied coordination compounds, a thin layer of the copper complex was deposited on a Si/SiO_2 native oxide substrate via drop casting and drying. This was used as the working electrode in an electrochemical cell (attached to a Cu disk), during the cyclic voltammetry experiments (Autolab PGstat128N potentiostat, 50 mV/s scan rate, starting at 0.5 V vs Ag/AgCl). 0.1 M tetramethyl-ammoniumbromide (Fluka) dissolved in ethanol was used as the supporting electrolyte, a Pt spiral wire was used as the counter electrode and a Ag/AgCl electrode was employed as a reference.

During coupled thermogravimetric (TG) analysis experiments, evolved gas analysis was performed *via* TG-mass spectrometry (MS) (TA instruments TGA Q 5000, Pfeiffer quadrupole MS, High-T Pt sample pan) and TG-differential scanning calorimetry (DSC) and Fourier transform infrared (FTIR) analysis (Mettler-Toledo TGA/DSC 1 coupled to a Bruker Vertex 70, alumina 70 µL cup). TG-MS measurements yield ion currents for all the selected m/z values (0.1 s per m/z time resolution, detector sensitivity of ch1000, balance gas flow 10 mL/min N_2, sample gas flow 35 mL/min N_2) and time-resolved infrared spectra could be obtained via TG-FTIR (ranging between 4000 and 600 cm^{-1}, 4 cm^{-1} resolution) complemented by Gram-Schmidt plots integrating all the signals in a selected wavenumber range.

Single crystal XRD measurement data were collected at -173 °C, on a Rigaku Oxford Diffraction Supernova Dual Source (Cu at zero) diffractometer equipped with an Atlas CCD detector using ω scans and CuK_α (λ = 1.54184 Å) radiation, or MoK_α (λ = 0.71073 Å) radiation. The patterns were interpreted and integrated with CrysAlisPro software [24]. Using Olex2 [25], the structures were solved by direct methods using the ShelXS structure solution program and refined by full-matrix least-squares on F^2 using the ShelXL software package [26,27]. Non-hydrogen atoms were anisotropically refined and the hydrogen atoms in the riding mode and isotropic temperature factors fixed at 1.2 times U(eq) of the parent atoms (1.5 times for methyl and hydroxyl groups). *In-situ* XRD measurements were performed, using a Bruker D8 Discovery with an experimental heating chamber, applying a 10 °C/min heating rate under He atmosphere.

The employed crystal structures in the paper at hand include CCDC 1132520 (CUFORM, copper formate [28]) and the copper formate pyridine complex, FORPCU [29], which was also redetermined and stored in the CSD (CCDC 1856775). Moreover, a novel crystal structure could be added to the database (CCDC

1856776). The supplementary crystallographic data for this paper can be obtained free of charge via [30].

X-ray absorption spectroscopy (XAS) was performed during measurement campaigns, using the DUBBLE-beamline, at the European Synchrotron radiation facility (ESRF-Grenoble), and the ROCK beamline at the Source Optimisée de Lumière d'Energie Intermédiaire de LURE (SOLEIL, Saint-Aubin) synchrotron facility. The BM26A at DUBBLE (Dutch-Belgian Beamline) features a bending magnet beamline, which was operated at the Cu K-edge (8979 eV) in transmission geometry ranging from 8779 eV up to 9679 eV with a 5 eV spacing just before (-20 eV) the edge, 0.3 eV in the edge region and a constant k spacing (0.05 $Å^{-1}$) from 20 eV after the Cu edge. The X-ray energy was selected, using a double Si(111) crystal monochromator in fixed-exit mode. Data were collected at RT and at liquid nitrogen temperature (-196 °C) in a closed cycle N_2 cryostat to reduce the damping of EXAFS oscillations related to thermal vibrations. The powder samples and references were diluted with boron nitride (Sigma-Aldrich, 98%, < 1µm) and pressed in circular pellets (1.2 cm^2 surface, pressure setting 40 kN/m^2, for 5 minutes) in such a way that the total number of absorption lengths was equal to 1. All spectra were recorded using an Ar/He (ratio 20/80) filled ionization chamber. Subsequently, the *in-situ* measurements were performed during heating from RT up to 400 °C with a heating rate of 2 °C/min, in He atmosphere in a dedicated microtome cell available at the ESRF sample environment laboratory. As copper powder was formed after all measurements in He, the resulting Cu spectrum was used as an internal reference for energy calibration and alignment between different samples. The occurrence of beam damage was evaluated by taking spectra for 30 minutes on the same measurement spot and comparing data. The data were aligned using the Athena® software package [31], deglitched and fitted with k^3 weighing scheme using the Viper® software [32] after applying a 'through the knots' background subtraction from 3.0 up to 12.5 $Å^{-1}$. The amplitude reduction factor S_0 was set to 1. The fitting models were constructed by converting reported crystallographic structures (in case of $Cu(HCOO)_2$ [28], $Cu(pyr)(HCOO)_2$ [33]), re-measured (in case of $Cu(pyr)_2(HCOO)_2$ [29]) or newly determined '.CIF' files ($Cu(en)_2(HCOO)_2$) with the Artemis® software to cluster the structure to finite dimensions (longest path length 6 Å) and subsequently running the FEFF7 code to determine the scatting paths and their relative contribution. The E_0 values were chosen to be the first maximum of the derivative spectra dµ(E)/dE and similar positive E-shifts were found during all fitting procedures (7.5 ± 2.0 eV).

The ROCK beamline at SOLEIL is especially designed for Quick-EXAFS *in-situ* measurements, using an oscillating channel-cut-crystal monochromator capable of covering a typical EXAFS spectrum in a sub-

second timeframe by selecting a certain angular amplitude $\Delta\theta$ around a fixed Bragg angle θ_B. The technical details on the working principle of the monochromator are described by Briois et al. [34,35]. The samples and references were measured in transmission mode between 8650 eV and 10200 eV, with an energy resolution of 0.2 eV between 8950 eV and 9872 eV, collecting a single scan every 0.25 s. The spectra at RT were obtained by summing 500 measurements to reduce the signal/noise ratio. Likewise, the data quality of the *in-situ* measurements during the temperature profile could be improved by summation of 12 subsequent measurements (time resolution = 6 s, giving rise to a thermal resolution of 0.5 °C in 5 °C/min heating ramp measurements). Energy calibration and alignment was performed by simultaneously measuring a copper foil reference. The Normal gui graphical interface available at the beamline was used for normalization and energy calibration using the 'pivot spectrum' for all the experiments. The samples were diluted with boron nitride (BN) to have an edge jump of approximately 1, and the powder mixture was gently pressed in a stainless steel sample holder composed of graphite foil sealing. After the recording of RT spectra, the samples were heated up to 300 °C, with a 2 °C/min or 5 °C/min heating rate in He atmosphere in a home-made oven described in [36].

Statistical data treatment

On the normalized and energy aligned XAS data matrices tracking the *in-situ* reduction, a principal component analysis (PCA) was performed. The purpose of this algorithm is to transform a high-dimensional dataset into a smaller-dimensional subspace expressing most of the variance of the original data set. The data reduction is based on analysis of variance and is well documented and frequently applied in QXANES/QEXAFS studies [37-39]. By orthogonal transformation, PCA converts the set of m experimental data into a set of m orthogonal eigenvectors, also called loadings, which are by construction linearly uncorrelated. Judging by the structure of the loading matrix (in other words the shape of the eigenvectors as a function of energy) and considering the variance explained by each eigenvector, a decision on the number of components mandatory for explaining most of the variance contained in the data set recorded during *in-situ* reduction is made. The eigenvalues (also called scores) associated with their respective eigenvectors account for the contribution to the total variance since the variance is the square of the eigenvalue (usually visualized in scree plots which is a representation of the eigenvalues sorted in descending order from the first one which explains the greatest variance of the loading matrix to the m ones). Moreover, the number of necessary components can be estimated by looking at the trajectory analysis of scores for the data set ordered along the reaction coordinates axis,

herein the time. This process is illustrated for the $Cu(hex)_2(HCOO)_2$ sample in supporting info S1. Herein the 'Singular Value Decomposition' algorithm, available in Matlab platform and customly scripted in order to offer all the loading, scree or trajectory plots necessary for decision, was used. Subsequently, using the PCA information about the number of relevant spectra explaining the variance of the data set, the multivariate curve regression with alternating least squares (MCR-ALS) algorithm [40] is used for extracting the absorption spectra of chemical species involved in the reaction and their concentration profiles from the experimental data set. The MCR-ALS method operates an alternating minimization of the differences between the experimental data set and the reconstructed data matrix equal to the product of the matrix of concentration and of the pure spectra of the components under the action of suitable chemically or physically meaningful constraints. Herein the constraints are the non-negativity assumed for both the spectra and concentration profiles, together with the closure of concentrations leading to verify that the sum of concentrations of Cu species involved in the reaction equals to 100% closure and with the unimodality behaviour of concentration imposing a single maximum per concentration profile. When the convergence criterion related to the standard deviance of the residuals versus the experimental data (s = 0.01) is fulfilled, two matrices can be extracted which can be visualized as follows: one showing the pure XAS spectra of the species present during the *in-situ* reduction and the other one their relative contribution as a function of temperature.

Linear combination analysis (LCA) was performed on calibrated and aligned XAS spectra in Athena® without E_0 fitting. The Linear combination analysis includes reference spectra which were calibrated manually using a Cu foil internal standard spectrum.

Results and Discussion

The decreasing reduction temperature upon alkylamine coordination of copper formate, as witnessed before [10-12], is confirmed and represented in figure 2. The decomposition onset of ortorhombic α-copper formate anhydrate is situated around 205 °C, coinciding with the conversion to metallic copper in inert atmosphere. No mass loss below 200 °C was detected, confirming the anhydrous nature of the freshly synthesized copper formate.

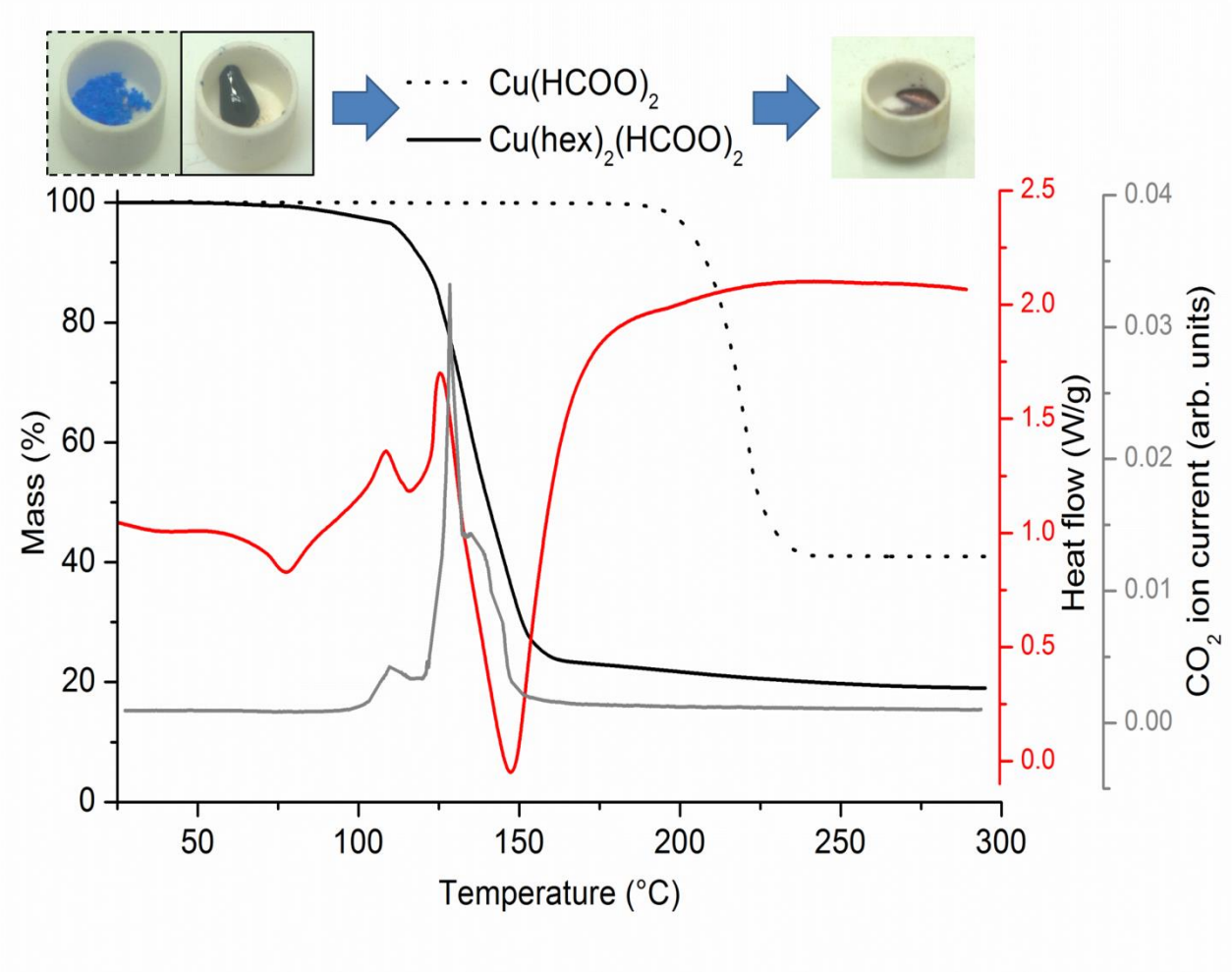

Figure 2: TGA (black curves) of copper formate and its hexylamine complex, together with a simultaneously recorded DSC signal (red, exo-up) and evolved carbon dioxide detection using mass spectroscopy (grey) for the hexylamine adduct. The images on top macroscopically demonstrate the succesful reduction to metallic copper.

Next to the neat copper formate, the thermogram of the copper hexylamine formate complex is plotted, undergoing its *in-situ* reduction at a significantly lower temperature (onset around 120 °C). Before that, a limited weight loss (approx. 2%) coinciding with an endothermic signal in the DSC at 79 °C takes place, related to residual ethanol evaporation. Both the copper formate and its hexylamine adduct were dried in vacuum conditions, rendering the assertion of the catalyzing water-molecule effect [14] unlikely in this system. Just before the start of the decomposition, a second endothermic peak can be distinguished, ascribed to the melting of the complex, coinciding with its *in-situ* reduction. The decomposition from the Cu(II) to the Cu(0) state seems to proceed in two distinct steps: the first is connected with an exothermic

peak whereas the second step clearly exhibits an endothermic behavior. Coupled TG-MS and TG-FTIR measurements point out that the hexylamine evolves only during the last stage of the reduction mechanism (see supporting info S2 and S3). Moreover, the carbon dioxide evolution is tracked and a sharp peak together with a pronounced shoulder shifted to higher temperatures is observed (figure 2 and supporting info S3). In other words, both the DSC and the evolved gas analysis strongly suggest a stepwise decomposition mechanism, possibly involving a Cu(I) intermediate, as the consecutive oxidation of the two present formate anions to carbon dioxide endorses this hypothesis.

Up to now, literature explanations on the reduction temperature shift only focus on the Cu(II) species or structure and ligand properties. However, an extensive investigation of basic Cu(II)-complex structure related properties (figure 3) shows that there is no simple correlation to be found between the decomposition temperatures (differential thermogravimetric analysis maxima) and parameters such as the (Cu-O) bond distance between the copper(II) center and the formate anion. The same applies for the relation between the decomposition temperature and the measured reduction potential (figure 3 and supporting information S4). The electron donating amine groups even lower the measured copper(II) reduction potential, which can be intuitively interpreted as an extra obstruction for low-temperature *in-situ* reductions.

Although the reducing properties of alkylamines at elevated temperatures are postulated in several studies (especially in the preparation of noble metal particles) [41,42], the synthesis of pure metallic copper could not be conducted with amines as the only reducing agent. Moreover, it is clearly stated that the role of alkylamines in copper particle synthesis is limited to solvent or dispersing agent in the presence of stronger reducing agents such as hydrogen gas, formate, carbon monoxide or oxalate [43]. Claims in literature [10,16,44] which directly correlate the in-situ reduction temperature to reducing properties of amines or the ease of CO_2 evolution can therefore be considered as incomplete simplifications. If the shift of the *in-situ* reduction temperature was solely related to the direct coordination of copper(II) to electron-donating amine groups, it would have to be expected that the ethylene-diamine reference compound would exhibit the lowest decomposition temperature due to the four-fold occupation of coordination positions by the amine groups (see figure 3). The experimental results clearly contradict this hypothesis.

However, it is also well known that the coordination geometry can affect the reduction potential, due to a changing structural preference between Cu(II) and Cu(I) species [45,46]. As demonstrated in figure 3, the complex with the highest electrochemical cathodic reduction potential (the anhydrous copper

formate), is characterized by the highest *in-situ* reduction temperature, and no systematic order is found for the other complexes. In addition, a correlation between the reduction temperature and the (Cu-O) bond length (equatorial(eq) or axial(ax)) with the reducing formate cannot be extracted. In concordance with the above arguments, still no simple relation between the Cu(II) coordination structure and the decomposition temperature can be found at first sight: in $Cu(hex)_2(HCOO)_2$ and $Cu(en)_2(HCOO)_2$, Cu(II) is found to be in its favored, very stable tetragonally distorted octahedral environment (figure 3, supporting info S5). The anhydrous orthorhombic α-copper formate is characterized by a square pyramidal coordination polygon network and the Cu(II) centers reside in trigonal bypiramid chains in the pyridine-based complexes (figure 3, supporting info S5). The last two environments are considered less stable for Cu(II), but their *in-situ* reduction temperatures are the highest (α-$Cu(HCOO)_2$) and the lowest ($Cu(pyr)_2(HCOO)_2$) of this study. Therefore, it can be deduced that the structures of the Cu(II) species have to be seen in relation with their respective Cu(I) intermediates to rationalize the differences in *in-situ* reduction temperatures.

	XRD	EXAFS	Selected properties	
Copper formate	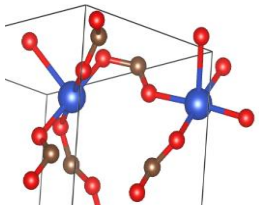	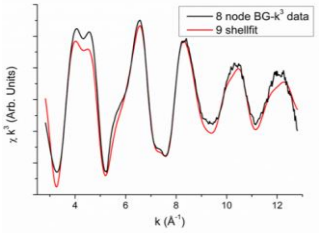	$(Cu-O)_{eq}$ XRD	1.93 – 1.97 Å
			$(Cu-O)_{ax}$ XRD	2.41 Å
			$(Cu-O)_{eq}$ EXAFS	1.94 – 1.97 Å
			$(Cu-O)^{ax}$ EXAFS	2.17 – 2.40 Å
			$T_{reduction}$	219 °C
			U_{red} vs Ag/AgCl	- 0.31 V
(pyr) complex	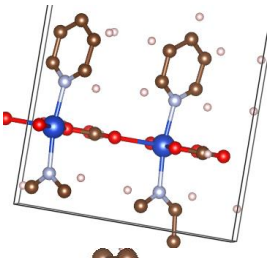	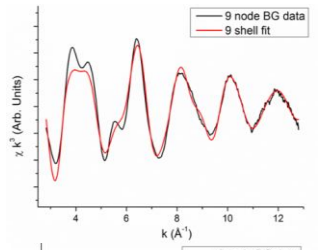	$(Cu-O)_{eq}$ XRD	1.95 – 1.99 Å
			$(Cu-O)_{ax}$ XRD	2.27 Å
			$(Cu-O)_{eq}$ EXAFS	1.92 – 2.02 Å
			$(Cu-O)^{ax}$ EXAFS	2.39 – 2.49 Å
			$T_{reduction}$	128 °C
			U_{red} vs Ag/AgCl	n.a.
(en) complex	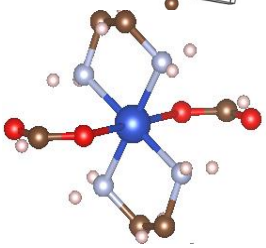	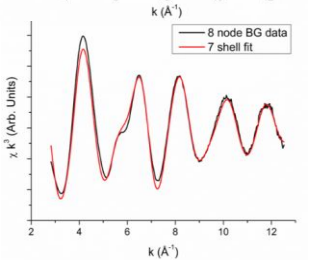	$(Cu-O)_{eq}$ XRD	n.a.
			$(Cu-O)_{ax}$ XRD	2.47 Å
			$(Cu-O)_{eq}$ EXAFS	n.a.
			$(Cu-O)^{ax}$ EXAFS	2.65 – 2.74 Å
			$T_{reduction}$	176 °C
			U_{red} vs Ag/AgCl	- 0.81 V
(hex) complex	No single crystals could be obtained	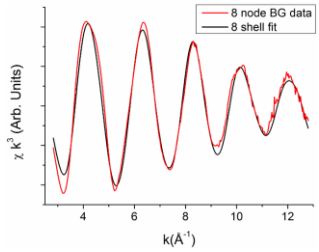	$(Cu-O)_{eq}$ XRD	n.a.
			$(Cu-O)_{ax}$ XRD	n.a.
			$(Cu-O)_{eq}$ EXAFS	1.98 – 1.99 Å
			$(Cu-O)^{ax}$ EXAFS	2.48 – 2.54 Å
			$T_{reduction}$	147 °C
			U_{red} vs Ag/AgCl	- 0.83 V

Figure 3: overview of the investigated copper(II) reference compounds and the $Cu(hex)_2(HCOO)_2$ MOD ink, based on single crystal XRD measurements for the crystalline reference compounds, EXAFS structure determination (see also supporting info S5), thermogravimetric analysis (supporting information S6) and cyclic voltammetry (supporting info S4). The crystal structures of the $Cu(HCOO)_2$ and (pyr) complex were already reported before [28,29]. The latter structure was redetermined (CCDC1856775) whereas the (en) structure is new to the CSD (CCDC1856776).

The copper complex structure during the reduction can be directly probed using *in-situ* XAS. The shift of the rising edge position (XANES) will supply immediate evidence on the oxidation state of the copper during the thermal degradation, whereas the shape of the edge holds valuable information on the coordination symmetry. For example, the typical XANES pre-edge feature related to electric dipole-forbidden 1s → 3d transitions unambiguously points to the presence of Cu(II) species [47,48]. Moreover, the derivative XANES shape confirms the tetragonally distorted octahedral coordination geometry (D_{4h},

axial elongation) for the $Cu(hex)_2(HCOO)_2$ and $Cu(en)_2(HCOO)_2$ compounds, giving a further indication of the magnitude of the distortion for both complexes [49] (supporting info S7). In addition, the extended fine structure in the EXAFS energy range can be analyzed to uncover the first coordination shells of the occurring intermediates. Upon quick inspection of the stacked *in-situ* XANES spectra of the $Cu(hex)_2(HCOO)_2$ MOD ink complex, a clear step-wise profile can immediately be recognized (figure 4). In the range between 80 – 100 °C, a distinct edge transformation occurs, taking the form of a characteristic Cu(I) XANES spectrum with an intense pre-edge resonance in the rising edge. On increasing the temperature further, the sharp Cu(I) pre-edge again disappears and Cu(0) is formed. PCA confirms the presence of 3 different species to account for 99.998% of the system's variance, and the result after MCR-ALS iteration is displayed in figure 4 as well. The 3 different species involved in the reduction correspond to a different Cu oxidation state and the related concentration profiles confirm the Cu(II) → Cu(I) → Cu(0) stepwise reduction. As hexylamine only evolves in the last step of the decomposition mechanism, the intermediate is hypothesized to be $Cu(hex)_2(HCOO)$.

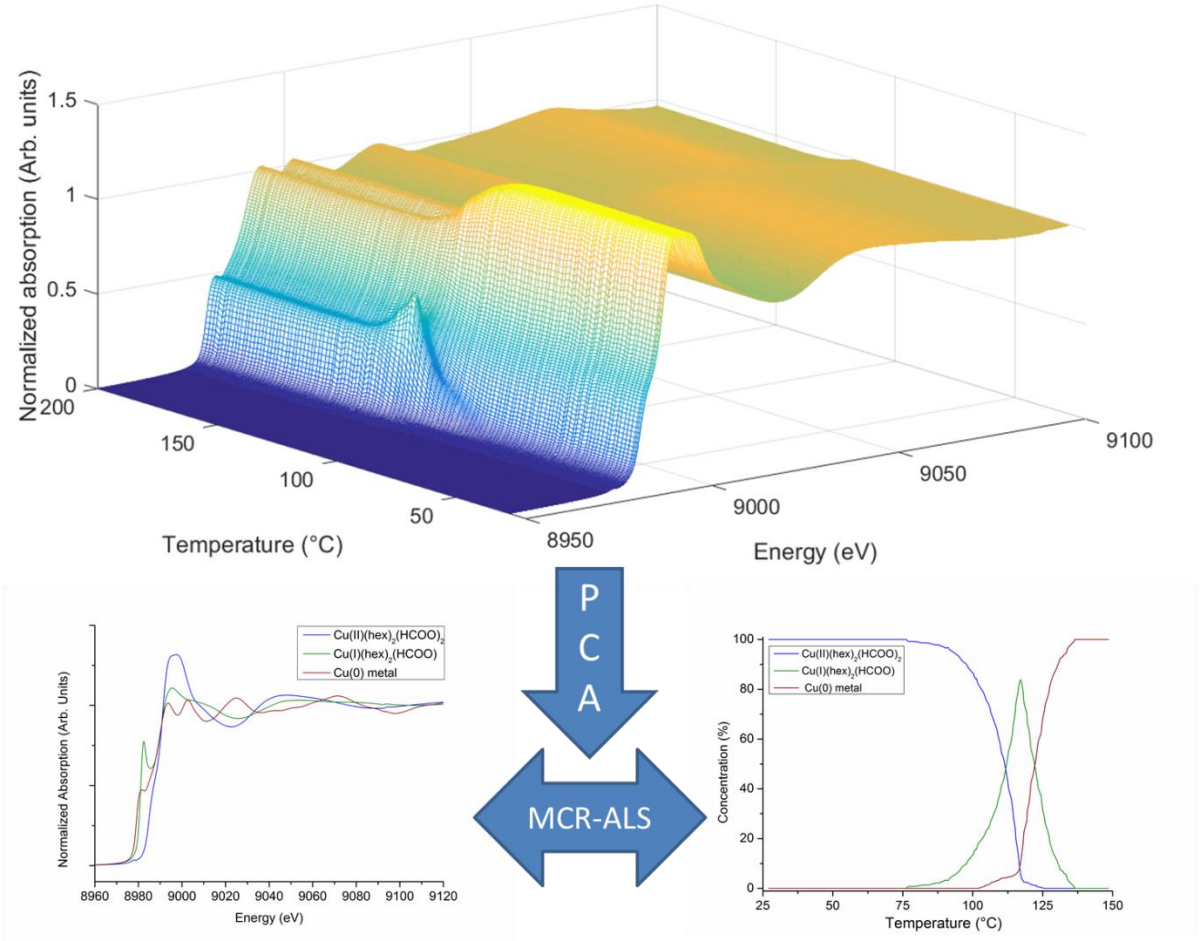

Figure 4: overview of a reduced in-situ XAS dataset (showing 1 spectrum out of 3, top), which was treated with the PCA algorithm to determine the number of components involved in the reaction (see supporting info S1), herein evaluated to 3 and the use of MCR-ALS allows to determine the 3 present 'pure' copper components (left side) and their respective concentration profiles (right side). Multiplication of both 2 dimensional representations yields a close approximation of the observed 3D in-situ measurement. A more detailed comparison between the raw and reconstructed data can be found in supporting info S8.

To gain supplementary insights into the *in-situ* reduction mechanism, the EXAFS spectra of the isolated MCR-ALS components are fitted. The structure of the starting compound $Cu(hex)_2(HCOO)_2$ was already determined before (figure 3 and supporting info S5), and a similar fitting procedure using a Cu(I) model yields the structures shown in figure 5. The structural model is build based on observations from other experimental techniques (TG-MS and TG-FTIR: the presence of a single formate and two hexylamines) and the measurement of Cu(I) reference compounds such as Cu_2O. The trigonal coordination for the Cu(I) intermediate complex is fully confirmed by the XANES pre-edge intensity and general shape [50], whereas the formation of metallic copper is confirmed by *in-situ*-HT-XRD (figure 5). The stable tetragonally distorted octahedral Cu(II) species is thus converted into a trigonal Cu(I) intermediate before reducing further to the metallic state.

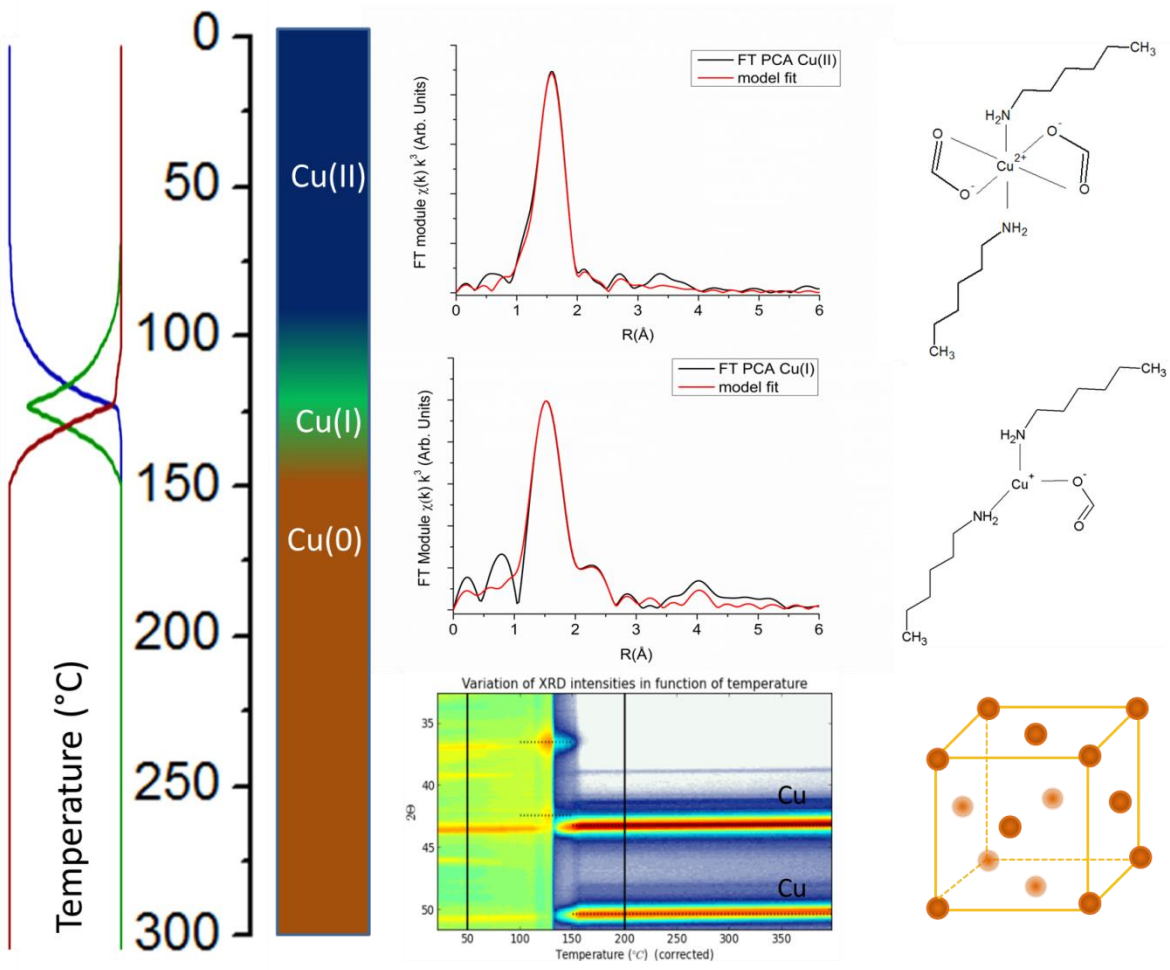

Figure 5: the in-situ reduction of Cu(hex)$_2$(HCOO)$_2$, consisting out of a stepwise Cu(II) → Cu(I)→ Cu(0) transition according to the displayed concentration profile on the left hand side. The intermediate Cu(I) and final Cu(0) structures are determined via EXAFS, XANES and XRD analysis, giving meaning to the observations in coupled TGA-MS and TGA-FTIR analysis.

In order to rationalize the temperature shift upon amine coordination, a bigger framework of similar analyses on the above mentioned reference structures is presented in figure 6. For the most thermolabile Cu(pyr)$_2$(HCOO)$_2$ complex, a four-step decomposition is found involving a Cu(II) intermediate (detailed PCA-MCR-ALS in supporting info S9). The transition between these two Cu(II) species can also be observed macroscopically due to a color change (blue to green) and in TGA measurements (supporting information S6 and S10), corresponding to the loss of one pyridine molecule per copper center, forming a Cu$_2$(pyr)$_2$(HCOO)$_2$ dimer [33,51]. It is very remarkable that the intermediate copper (II) complex and the Cu(I) species show great structural similarities, possibly favoring a smooth Cu(II) → Cu(I) reduction mechanism at low temperatures. The structural determination of both

complexes via EXAFS can be seen in supporting information S11. Also for the $Cu(en)_2(HCOO)_2$ and the α-$Cu(HCOO)_2$ salt, the occurrence of a short living Cu(I) intermediate is evidenced. However, in both cases, the Cu(I) intermediate is so unstable that a 100% pure spectrum cannot be isolated by the MCR-ALS algorithm. The presence of the Cu(I) species in the *in-situ* reduction is therefore proven via linear combination analysis using a similar Cu(I) spectrum as a reference (supporting information S12). The failure to isolate a pure Cu(I) species by MCR-ALS is assumed to be linked to an intrinsic limitation of the method, known as rank deficiency limitation, which can appear when two distinct chemical species evolve concomitantly, their resulting behavior in the experimental data appears as merged in a single spectral component

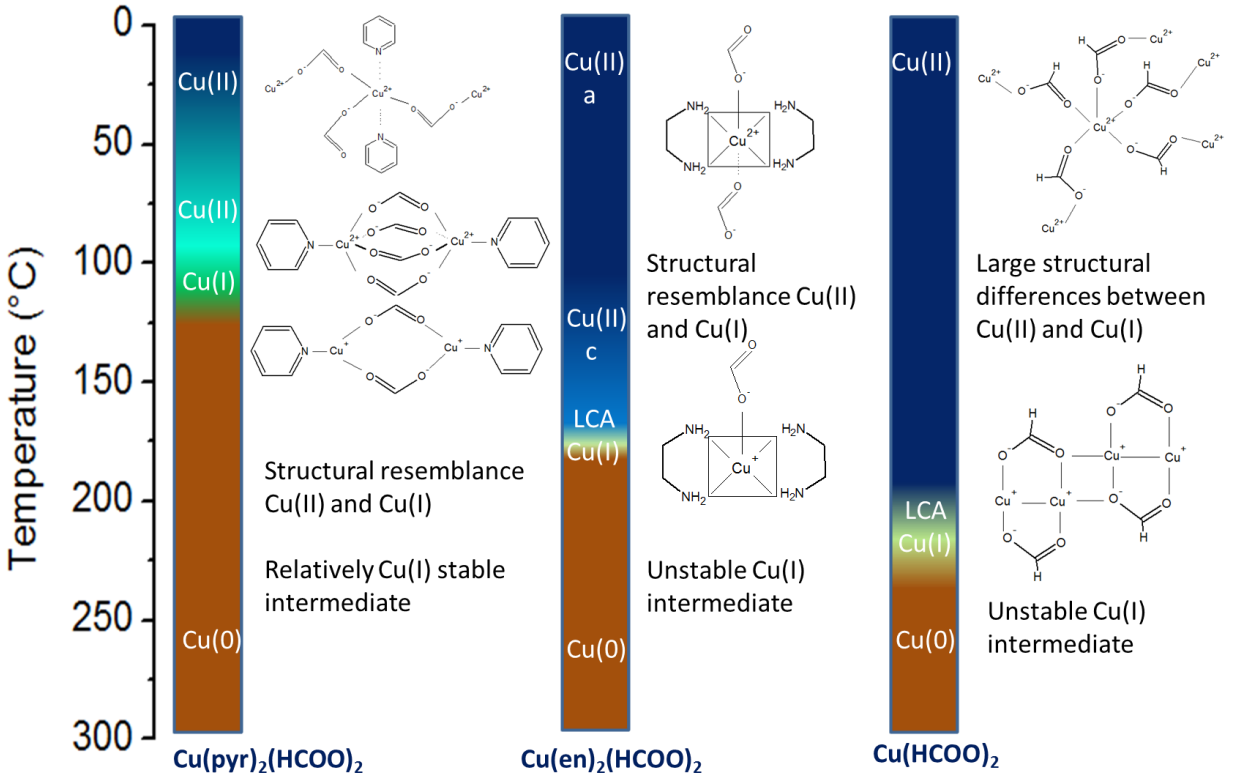

Figure 6: overview of the in-situ reduction mechanisms of the reference compounds, supplying the rational for the observed temperature shift. Next to the evolution of the different copper oxidation states as a function of the temperatures, the fitted EXAFS models are depicted. For the Cu(I) intermediates of $Cu(en)_2(HCOO)_2$ and α-$Cu(HCOO)_2$, the assumed structures are based on indirect measurements (coupled TGA) and literature.

The higher *in-situ* reduction temperature and the instability of the occurring Cu(I) intermediate in the $Cu(en)_2(HCOO)_2$ complex can be explained as follows: both ethylenediamine ligands only evolve in the last step of the reduction in the Cu(I) → Cu(0) process (see supporting info S13 for TGA-MS). Given the large tetragonal distortion in the Cu(II) complex, a quasi-square planar coordination geometry is imposed on the Cu(I) structure, which is highly disfavored due to its closed d^{10} shell electron configuration [52,53]. In other words, to end up as metallic copper, the $Cu(en)_2(HCOO)_2$ complex needs to surpass an energetically unfavorable intermediate, therefore requiring a higher temperature. For the anhydrous α-copper formate (detailed MCR-ALS XANES in supporting info S12), the situation is even more pronounced: not only is its Cu(I) intermediate likely to be a square planar dimeric Cu(I) chainlike structure, as indirectly observed in literature [54] and in concordance with the well-known structure of similar Cu(I)carboxylates [55,56]. Moreover, the strong network of carboxylate bridges in the α-$Cu(II)(HCOO)_2$ structure needs to be broken apart completely, not only to end up with the metallic Cu(0) fcc structure, but also to form the unstable Cu(I) dimers which have little in common with their parent structure. The combination of having both an unstable Cu(I) intermediate, due to its coordination geometry, and little structural resemblance between the Cu(II) and Cu(I) species, causes a high *in-situ* reduction temperature.

In general, this study shows the great importance of a detailed structural study to account for the ability of MOD ink complexes to be reduced at low temperatures. The occurrence of the Cu(I) intermediate imposes an important design rule for copper MOD inks: its stability and structural resemblance to the Cu(II) precursor is key for attaining a low-temperature decomposition. It enables us to understand why the decomposition of the $Cu(hex)_2(HCOO)_2$ MOD ink falls in a suitable temperature range to deposit metallic copper on sensitive substrates such as PET (see supporting info S14) or paper, whereas the $Cu(en)_2(HCOO)_2$ complex would not be a good candidate. The occurrence of a Cu(I) intermediate and its essential influence on the temperature shift of the *in-situ* reduction mechanism can be even strengthened further by the observation that the reduction temperature of nickel formate to metallic nickel cannot be shifted to the same extent via amine coordination [57] (supporting information S15), due to the lack of Ni(I) chemistry. Once more, this illustrates that the intermediate Cu(I) complexes' formation needs to be facilitated as much as possible in order to reach an as low as possible processing temperature. In order to achieve this facilitation, the Cu(I) complexes formed during the transformation of the Cu(II) precursor complex into the final Cu metal, need to show as high as possible structural resemblance to the Cu(II) parent and need to have a favorable stability, as determined by their coordination geometry.

Conclusion

In summary, it was shown that all the *in-situ* reduction mechanisms of copper formate related coordination compounds proceed via a transient Cu(I)-intermediate. The presence of this intermediate has been directly detected via PCA-MCR-ALS analysis of *in-situ* XAS measurements, or has been verified with great certainty based on linear combination analysis. In addition, via an in-depth follow up of the complex structures of the $Cu(hex)_2(HCOO)_2$ MOD ink and a selection of reference compounds, it was inferred that the reduction temperature is related to two important factors. On the one hand, the relative stability of the Cu(I) intermediate itself, on the other hand the structural similarities between the respective Cu(II) and Cu(I) species along the thermal decomposition route. The revelation of these new explanatory variables shed a new light on the design of copper MOD inks for the development of printable flexible electronics.

Acknowledgements

The authors acknowledge F. Mattelaer and C. De Tavernier from the COCOON group at Ghent university for the in-situ HT-XRD measurements to support the findings based on the XAS data. Moreover, J. Maggen is acknowledged for performing the CHN analysis, B. Joos and G. Maino for the electrochemical experiments, and the DUBBLE and SOLEIL beam staff for their support during and after the measurement campaigns. Moreover, this work was supported by a public grant overseen by the French National Research Agency (ANR) as part of the “Investissements d’Avenir” program (reference : ANR10-EQPX45). Prof. Van Hecke thanks the Hercules Foundation (project AUGE/11/029 “3D-SPACE: 3D Structural Platform Aiming for Chemical Excellence”) and the Special Research Fund (BOF) – UGent (project 01N03217) for funding. Finally, the authors are grateful for the SIM-Met@link funding

References

1. Grouchko, M.; Kamyshny, A.; Mihailescu, C.F.; Anghel, D.F.; Magdassi, S. Conductive inks with a "built-in"mechanism that enables sintering at room temperature. *ACS Nano* **2011**, *5*, 3354-3359.
2. Tsai, C.Y.; Chang, W.C.; Chen, G.L.; Chung, C.H.; Liang, J.X.; Ma, W.Y.; Yang, T.N. A study of the preparation and properties of antioxidative copper inks with high electrical conductivity. *Nanoscale Res Lett* **2015**, *10*, 357.
3. Lim, S.; Joyce, M.; Fleming, P.D.; Aijazi, A.T.; Atashbar, M. Inkjet printing and sintering of nano-copper ink. *Journal of Imaging Science and Technology* **2013**, *57*, 1-7.
4. Schwartz, R.W.; Schneller, T.; Waser, R. Chemical solution deposition of electronic oxide films. *Comptes Rendus Chimie* **2004**, *7*, 433-461.
5. Marchal, W.; Vandevenne, G.; D'Haen, J.; Calmont de Andrade Almeida, A.; Durand Sola, M.A.; van den Ham, E.J.; Drijkoningen, J.; Elen, K.; Deferme, W.; Van Bael, M.K.*, et al.* Ultrasonically spray coated silver layers from designed precursor inks for flexible electronics. *Nanotechnology* **2017**, *28*, 215202.
6. Walker, S.B.; Lewis, J.A. Reactive silver inks for patterning high-conductivity features at mild temperatures. *Journal of the American Chemical Society* **2012**, *134*, 1419-1421.
7. Paquet, C.; Lacelle, T.; Deore, B.; Kell, A.J.; Liu, X.; Korobkov, I.; Malenfant, P.R. Pyridine-copper(ii) formates for the generation of high conductivity copper films at low temperatures. *Chemical communications* **2016**, *52*, 2605-2608.
8. Berner, U.; Widenmeyer, M. Solution-based processing of cu(in,ga)se2absorber layers for 11% efficiency solar cells via a metallic intermediate. *Progress in Photovoltaics: Research and Applications* **2014**, n/a-n/a.
9. Farraj, Y.; Smooha, A.; Kamyshny, A.; Magdassi, S. Plasma-induced decomposition of copper complex ink for the formation of highly conductive copper tracks on heat-sensitive substrates. *ACS applied materials & interfaces* **2017**, *9*, 8766-8773.
10. Choi, Y.H.; Hong, S.H. Effect of the amine concentration on phase evolution and densification in printed films using cu(ii) complex ink. *Langmuir* **2015**, *31*, 8101-8110.
11. Yabuki, A.; Tanaka, S. Electrically conductive copper film prepared at low temperature by thermal decomposition of copper amine complexes with various amines. *Materials Research Bulletin* **2012**, *47*, 4107-4111.
12. Xu, W.; Wang, T. Synergetic effect of blended alkylamines for copper complex ink to form conductive copper films. *Langmuir* **2017**, *33*, 82-90.
13. Kim, S.J.; Lee, J.; Choi, Y.-H.; Yeon, D.-H.; Byun, Y. Effect of copper concentration in printable copper inks on film fabrication. *Thin Solid Films* **2012**, *520*, 2731-2734.
14. Farraj, Y.; Grouchko, M.; Magdassi, S. Self-reduction of a copper complex mod ink for inkjet printing conductive patterns on plastics. *Chemical communications* **2015**, *51*, 1587-1590.
15. Yabuki, A.; Tachibana, Y.; Fathona, I.W. Synthesis of copper conductive film by low-temperature thermal decomposition of copper–aminediol complexes under an air atmosphere. *Materials Chemistry and Physics* **2014**, *148*, 299-304.
16. Shin, D.H.; Woo, S.; Yem, H.; Cha, M.; Cho, S.; Kang, M.; Jeong, S.; Kim, Y.; Kang, K.; Piao, Y. A self-reducible and alcohol-soluble copper-based metal-organic decomposition ink for printed electronics. *ACS applied materials & interfaces* **2014**, *6*, 3312-3319.
17. Galwey, A.K.; Jamieson, D.M.; Brown, M.E. Thermal decomposition of three crystalline modifications of anhydrous copper(ii) formate. *Journal of Physical Chemistry* **1974**, *78*, 2664-2670.

18. Mohamed, M.A.; Galwey, A.K.; Halawy, S.A. Kinetic and thermodynamic studies of the nonisothermal decomposition of anhydrous copper(ii) formate in different gas atmospheres. *Thermochimica Acta* **2004**, *411*, 13-20.
19. Lee, J.; Lee, B.; Jeong, S.; Kim, Y.; Lee, M. Microstructure and electrical property of laser-sintered cu complex ink. *Applied Surface Science* **2014**, *307*, 42-45.
20. Wang, B.Y.; Yoo, T.H.; Song, Y.W.; Lim, D.S.; Oh, Y.J. Cu ion ink for a flexible substrate and highly conductive patterning by intensive pulsed light sintering. *ACS applied materials & interfaces* **2013**, *5*, 4113-4119.
21. Araki, T.; Sugahara, T.; Jiu, J.; Nagao, S.; Nogi, M.; Koga, H.; Uchida, H.; Shinozaki, K.; Suganuma, K. Cu salt ink formulation for printed electronics using photonic sintering. *Langmuir* **2013**, *29*, 11192-11197.
22. Paquet, C.; Lacelle, T.; Liu, X.; Deore, B.; Kell, A.J.; Lafreniere, S.; Malenfant, P.R.L. The role of amine ligands in governing film morphology and electrical properties of copper films derived from copper formate-based molecular inks. *Nanoscale* **2018**, *10*, 6911-6921.
23. Martin, R.L.; Waterman, H. Magnetic studies with copper(ii) salts. Part iv remarkable magnetic behaviour of copper(n) formate and its hydrates. **1959**, 1359.
24. Rigaku Oxford Diffraction (2015). CrysAlis Pro; Rigaku Oxford Diffraction, Yarnton, England
25. Dolomanov, O.V.; Bourhis, L.J.; Gildea, R.J.; Howard, J.A.K.; Puschmann, H. *Journal of Applied Crystallography* **2009**, *42*, 339-341.
26. Sheldrik, G.M. *Acta Crystallographica* **2008**, *A64*, 112-122.
27. Sheldrik, G.M. *Acta Crystallographica* **2015**, *C71*, 3-8.
28. G.A. Barclay, C.H.L.K. The crystal structure of anhydrous copper(ii) formate. **1961**, 3289.
29. Cartwright, B.A.; Couchman, L.; Skapski, A.C. A square pyramidam copper complex containing both monodentate and anti-syn bridging formate groups. *Acta Crystallographica* **1979**, *35*, 824-827.
30. Centre, t.C.C.D. Www.Ccdc.Cam.Ac.Uk/conts/retrieving.Html *12 Union road, Cambridge CB2 1EZ deposit@ccdc.cam.ac.uk*.
31. Ravel, B.; Newville, M. Thena, artemis, hephaestus: Data analysis for x-ray absorption spectroscopy using ifeffit. *Journal of synchrotron radiation* **2005**, *12*, 537-541.
32. Klementev, K.V. Package "viper (visual processing in exafs researches) for windows. *Nuclear Instruments and Methods in Physics Research Section A* **2000**, *448*.
33. Barquín, M.; Cocera, N.; González Garmendia, M.J.; Larrínaga, L.; Pinilla, E.; Torres, M.R. Acetato and formato copper(ii) paddle-wheel complexes with nitrogen ligands. *Journal of Coordination Chemistry* **2010**, *63*, 2247-2260.
34. Briois, V.; La Fontaine, C.; Belin, S.; Barthe, L.; Moreno, T.; Pinty, V.; Carcy, A.; Girardot, R.; Fonda, E. Rock: The new quick-exafs beamline at soleil. *Journal of Physics: Conference Series* **2016**, *712*, 012149.
35. Fonda, E.; Rochet, A.; Ribbens, M.; Barthe, L.; Belin, S.; Briois, V. The samba quick-exafs monochromator: Xas with edge jumping. *Journal of synchrotron radiation* **2012**, *19*, 417-424.
36. La Fontaine, C.; Barthe, L.; Rochet, A.; Briois, V. X-ray absorption spectroscopy and heterogeneous catalysis: Performances at the soleil's samba beamline. *Catalysis Today* **2013**, *205*, 148-158.
37. Calvin, S. *Xafs for everyone*. CRC Press - Taylor & Francis group Boca raton, 2013.
38. Rochet, A.; Baubet, B.; Moizan, V.; Pichon, C.; Briois, V. Co-k and mo-k edges quick-xas study of the sulphidation properties of mo/al2o3 and como/al2o3 catalysts. *Comptes Rendus Chimie* **2016**, *19*, 1337-1351.
39. Cassinelli, W.H.; Martins, L.; Passos, A.R.; Pulcinelli, S.H.; Santilli, C.V.; Rochet, A.; Briois, V. Multivariate curve resolution analysis applied to time-resolved synchrotron x-ray absorption

spectroscopy monitoring of the activation of copper alumina catalyst. *Catalysis Today* **2014**, *229*, 114-122.
40. de Juan, A.; Jaumot, J.; Tauler, R. Multivariate curve resolution (mcr). Solving the mixture analysis problem. *Analytical Methods* **2014**, *6*, 4964.
41. Salavati-Niasari, M.; Davar, F.; Mir, N. Synthesis and characterization of metallic copper nanoparticles via thermal decomposition. *Polyhedron* **2008**, *27*, 3514-3518.
42. Wang, D.; Li, Y. Effective octadecylamine system for nanocrystal synthesis. *Inorganic chemistry* **2011**, *50*, 5196-5202.
43. Mourdikoudis, S.; Liz-Marzán, L.M. Oleylamine in nanoparticle synthesis. *Chemistry of Materials* **2013**, *25*, 1465-1476.
44. Yonezawa, T.; Tsukamoto, H.; Yong, Y.; Nguyen, M.T.; Matsubara, M. Low temperature sintering process of copper fine particles under nitrogen gas flow with cu2+-alkanolamine metallacycle compounds for electrically conductive layer formation. *RSC Adv.* **2016**, *6*, 12048-12052.
45. Patterson, G.S.; Holm, R.H. Structural and electronic effects on the polarographic half-wave potentials of copper(ii) chelates. *Bioinorganic Chemistry A* **1975**, *4*, 257-275.
46. Ambundo, E.A.; Deydier, M.V.; Grall, A.J.; Aguera-Vega, N.; Dressel, L.T.; Cooper, T.H.; Heeg, M.J.; Ochrymowycz, L.A.; Rorabacher, D.B. Influence of coordination geometry upon copper(ii/i) redox potentials. Physical parameters for twelve copper tripodal ligand complexes. *Inorganic chemistry* **1999**, *38*.
47. Gaur, A.; Shrivastava, B.D. Speciation of mixtures of copper (i) and copper (ii) mixed ligand complexes by x-ray absorption fine structure spectroscopy. *Spectroscopy Letters* **2013**, *46*, 375-383.
48. Kim, W.B.; Lee, J.S. Quantitative xanes analysis of cuprous dibromide complex formed in the oxidative carbonylation of phenols. *Journal of Physical Chemistry B* **2003**, *107*, 9195-9202.
49. Frenkel, A.I.; Korshin, G.V.; Ankudinov, A.L. Xanes study of cu2+-binding sites in aquatic humic substances. *Environmental Science and Technology* **2000**, *34*, 2138-2142.
50. Kau, L.S.; Spira-Solomon, D.J.; Penner-Hahn, J.E.; Hodgson, K.O.; Solomon, E.I. X-ray absorption edge determination of the oxidation state and coordination number of copper. *Journal of the American Chemical Society* **1987**, *109*, 6433-6442.
51. Uekusa, H.; Ohba, S.; Saito, Y.; Kato, M.; Tokii, T.; Muto, Y. Structural comparison between dimeric copper(ii) formate and acetate in pyridine and urea adducts. *Acta Chrystallographica* **1989**, *C45*, 377-380.
52. Takeuchi, K.; Taguchi, H.O.; Tanigawa, I.; Tsujimoto, S.; Matsuo, T.; Tanaka, H.; Yoshizawa, K.; Ozawa, F. A square-planar complex of platinum(0). *Angewandte Chemie* **2016**, *55*, 15347-15350.
53. Albright, T.A.; Burdett, J.K.; Whangboo, M.H. *Orbital interactions in chemistry*. Wiley: Hoboken, 2013.
54. Edwards, D.A.; Richards, R. The mass spectra of copper(i) carboxylates. *Journal of Inorganic and Nuclear Chemistry* **1972**, *8*, 783-792.
55. Mounts, R.D.; Ogura, T.; Fernando, Q. Crystal structure of copper(i) acetate. *Inorganic chemistry* **1974**, *13*, 802-805.
56. Bazhanova, Z.G.; Tarasov, Y.I.; Kovtun, D.M.; Boltalin, A.I.; Novosadov, B.K.; Kochikov, I.V. Quantum-chemical study of the structure of copper (i) acetate and trifluoroacetate oligomers. *Journal of Structural Chemistry* **2008**, *49*, 810-827.
57. Yabuki, A.; Ichida, Y.; Kang, S.; Fathona, I.W. Nickel film synthesized by the thermal decomposition of nickel-amine complexes. *Thin Solid Films* **2017**, *642*, 169-173.

For table of contents only

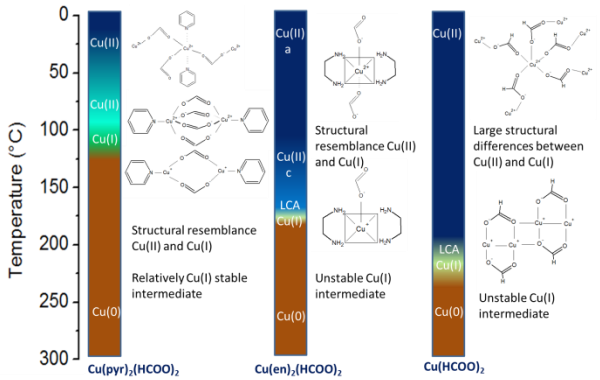

The Cu(I) intermediate structure and stability during decomposition defines whether the copper ink is thermally compatible with printing on plastics.